Electronic Supplementary Information

Solvent-induced assembly and photocatalytic properties of atomically precise tellurotungstate-templated Ag clusters

Jiwei Ning, Mengyun Zhao, Yuanyuan Dong*, Manzhou Chi, Yurui Li, Yeqin Feng*, Yun Qin, Hongjin Lv*, Guo-Yu Yang

MOE Key Laboratory of Cluster Science, Beijing Key Laboratory of Intelligent Molecular Materials and High-throughput Manufacturing, School of Chemistry and Chemical Engineering, Beijing Institute of Technology, Beijing 102488, P. R. China

Corresponding author. E-mail: dyy1111@bit.edu.cn; fyq@bit.edu.cn; hlv@bit.edu.cn

Experimental Section

Characterization. The FT–IR spectra were performed on a Bruker Tensor II spectrometer in the range of 4000–400 cm^{-1}. Solid-state UV–vis spectra were recorded on a Techcomp UV 2600 spectrophotometer at room temperature within the wavelength range of 220-800 nm. Powder XRD patterns were performed on a MiniFlex 600 diffractometer with a Cu-Kα X−ray radiation source. The X−ray Photoelectron Spectrum (XPS) was recorded on a PHI5000 Versaprobe III. Thermogravimetric analysis (TGA) was conducted using a STA 449 F3/F5 thermal analyzer at a heating rate of 10 ℃/min under a N_2 atmosphere, in the temperature range of 30 to 800 ℃. Photothermal measurements were performed using a Laser MGL-III-465nm-300mW system. The photothermal behavior of the sample was monitored using a thermal imaging camera (Fotric 326C). Infrared images and real-time temperature data were extracted from the video recordings using FLIR Tools software.

Single-Crystal X-ray Crystallography: Suitable single crystals of **Ag60** and **Ag46** were selected under an optical microscope and protected from decomposition by coating with Paratone-N oil. The crystals were then mounted on loops, and X-ray diffraction data were collected at 100 K on a Rigaku Oxford Diffraction XtaLAB Synergy diffractometer using Mo Kα radiation (λ = 0.71073 Å, graphite monochromator). All data processing steps, including collection, indexing, and unit-cell refinement, were conducted using the CrysAlisPro software suite. The structures were solved with the Olex2 and the SHELXT structure solution program using Charge Flipping[1] and refined with the SHLXL refinement package using Least Squares minimization.[2] All non-hydrogen atoms were refined anisotropically, while hydrogen atoms attached to carbon were placed in calculated positions and refined isotropically using a riding model. Appropriate geometric and anisotropic displacement parameter (ADP) restraints were imposed on the relevant atoms within the cluster. Some disagreeable reflections were omitted by OMIT orders. Crystal structure graphics were carried out by using Diamond 4 software. CCDC 2546840 and 2546839 provide the additional crystallographic data for **Ag60** and **Ag46**, respectively. The crystallographic data can be found from The Cambridge Crystallographic Data Centre via www.ccdc.cam.ac.uk/data_request/cif.

Bond valence sum (BVS) calculation: The BVS values were calculated by the expression for the variation of the length rab of a bond between two atoms a and b in observed crystal with valence Va.

$$Va = \sum exp\left(\frac{r_0 - r_{ab}}{B}\right)$$

where B is constant equal to 0.37 Å, r_0 is bond valence parameter for a given atom pair.[3]

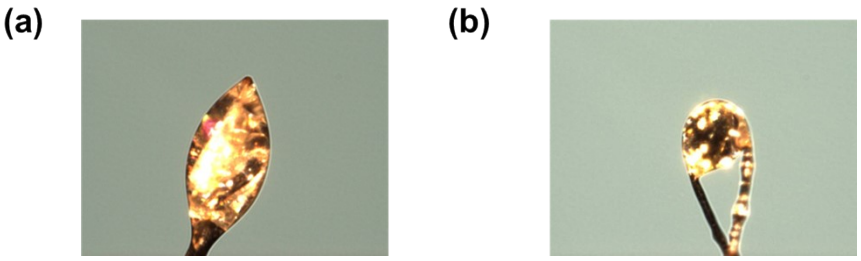

Fig. S1 Digital photograph of single crystal of (a) **Ag60** and (b) **Ag46**.

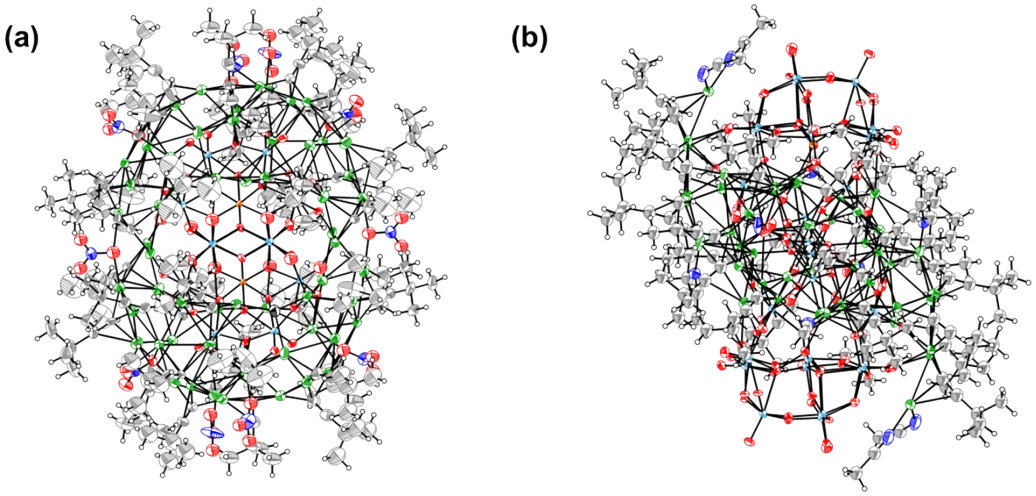

Fig. S2 A displacement ellipsoid plot of (a) **Ag60** and (b) **Ag46**. Non-H atoms are represented by ellipsoids at the 50% probability. Color codes: Ag, green; Te, orange; W, light blue; O, red; C, gray; N, dark blue; H, white.

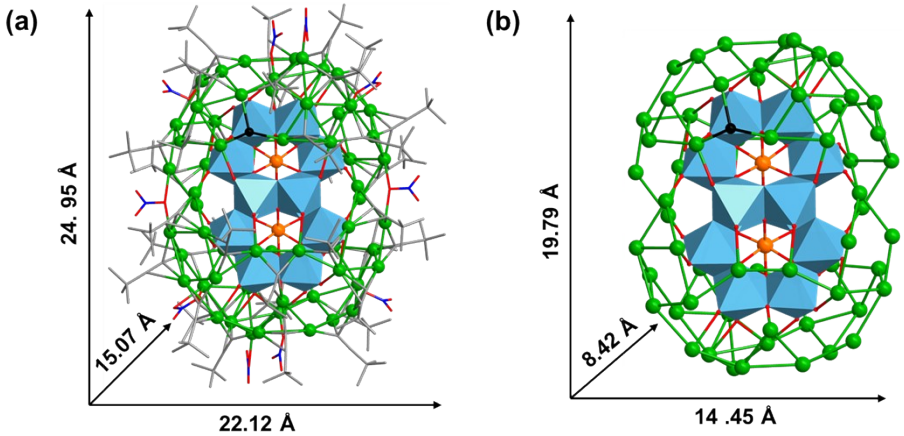

Fig. S3 X-ray structures and sizes of (a) **Ag60** cluster. (b) $(TeW_6O_{24})_2@Ag_{60}$ skeleton Color codes: Ag, green; Te, orange; W, light blue; O, red; C, gray; N, dark blue; $\{WO_6\}$, light blue polyhedron.

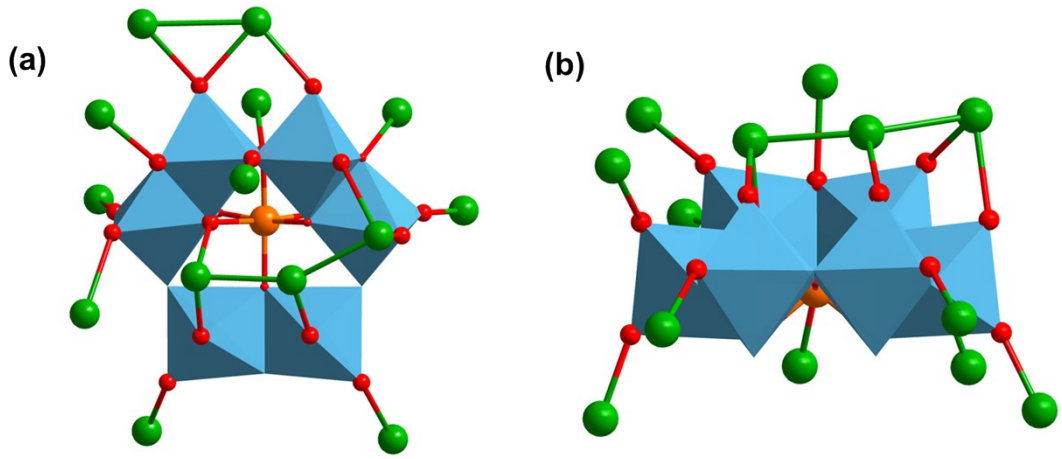

Fig. S4 (a) and (b) Coordination modes of the $[TeW_6O_{14}]^{6-}$ anion toward 14 silver atoms along two directions in **Ag60**, featuring both terminal and bridging O-atom coordination. Color codes: Ag, green; O, red; Te, orange.

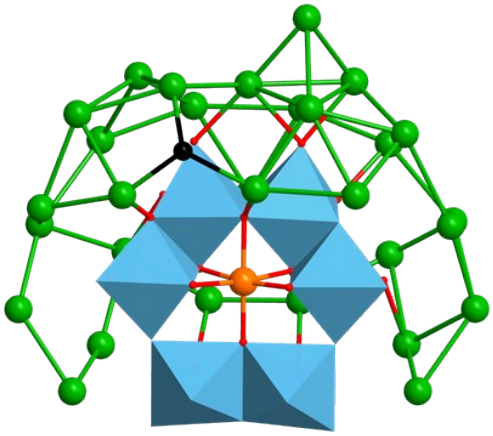

Fig. S5 $[(TeW_6O_{24})@Ag_{30}Cl]$ subunit. Color codes: Ag, green; O, red; Te, orange; Cl, black.

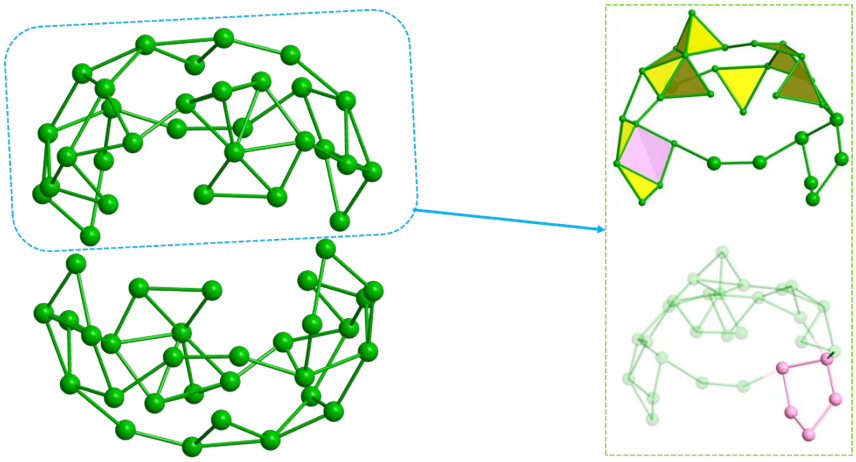

Fig. S6 The silver shell of the **Ag60** cluster. Left: overall structure; right: Ag triangles (yellow), squares (purple), and pentagons (pink). Color codes: Ag, green, pink.

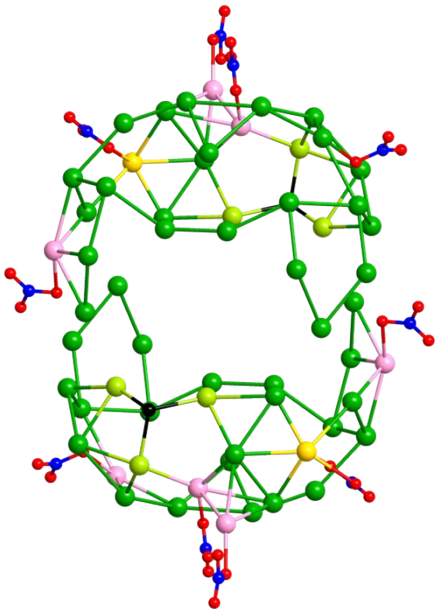

Fig. S7 The coordination modes of the Cl^- and NO_3^- ions within the **Ag60** cluster. Color codes: Ag, green, pink, yellow, yellow-green; O, red; N, dark blue; Cl, black.

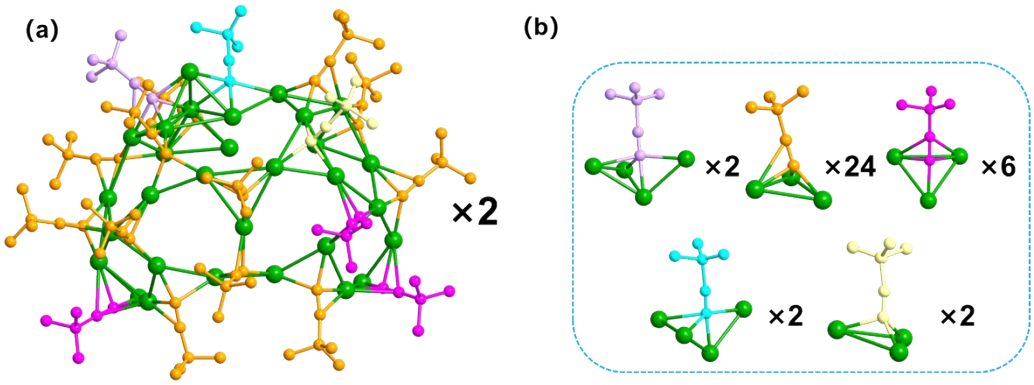

Fig. S8 (a) The 18 ^{t}BuC≡C$^-$ ligands on the periphery of **Ag_{30}** shell. (b) the coordination modes of 36 ^{t}BuC≡C$^-$ ligands: 2 in μ_4-η^1:η^1:η^1:η^1, 24 in μ_3-η^1:η^1:η^2, 6 in μ_3-η^1:η^2:η^2, 2 in μ_4-η^1:η^1:η^1:η^1, 2 in μ_3-η^1:η^1: η^1. Color codes: Ag, green; C, pink, yellow, purple, sky blue, pale yellow.

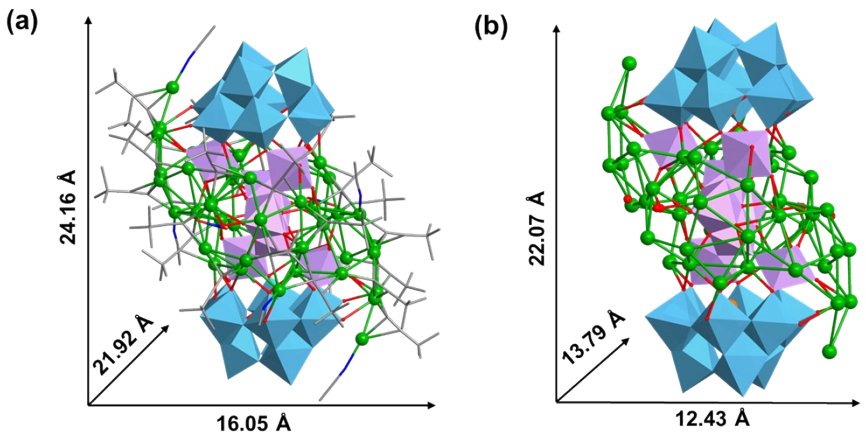

Fig. S9 X-ray structures and sizes of (a) **Ag46** cluster. (b) $(TeW_{13}O_{46})_2$@Ag_{46} skeleton. Color codes: Ag, green; Te, orange; W, light blue; O, red; C, gray; N, dark blue; $\{WO_6\}$, light blue polyhedron, purple polyhedron.

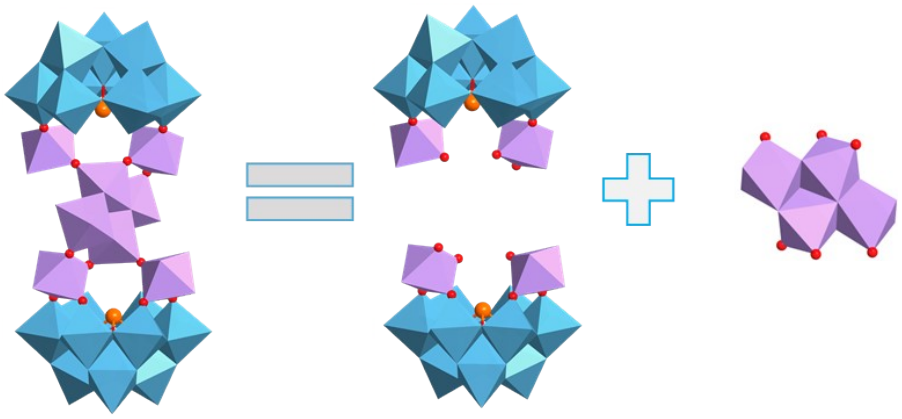

Fig. S10 The structure is composed of two $[TeW_{11}O_{41}]^{12-}$ units connected by shared terminal oxygen atoms (highlighted) from a central planar $[W_4O_{16}]^{8-}$ segment. Color codes: Te, orange; W, light blue; O, red; $\{WO_6\}$, light blue polyhedron, purple polyhedron.

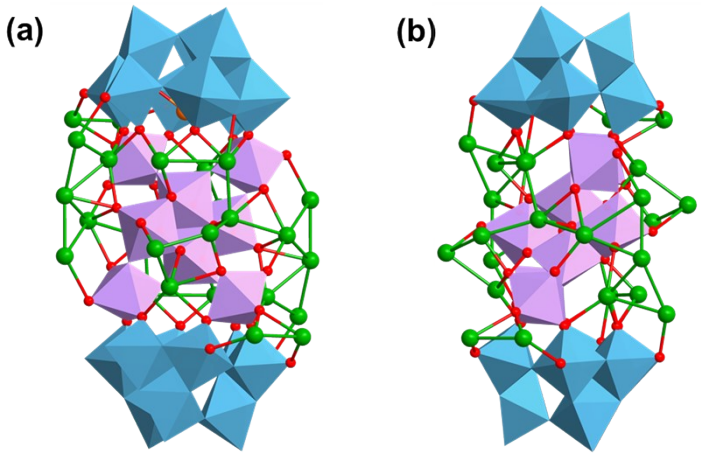

Fig. S11 (a) and (b) The coordination modes of dumbbell-shaped $[Te_2W_{26}O_{92}]^{20-}$ anion toward 24 silver atoms along two directions in **Ag46**. Color codes: Ag, green; O, red; Te, orange; $\{WO_6\}$, light blue polyhedron, purple polyhedron.

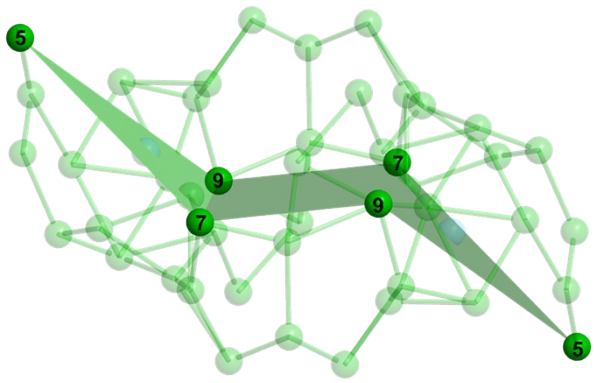

Fig. S12 The overall framework of the silver skeleton adopts a chair-like conformation.

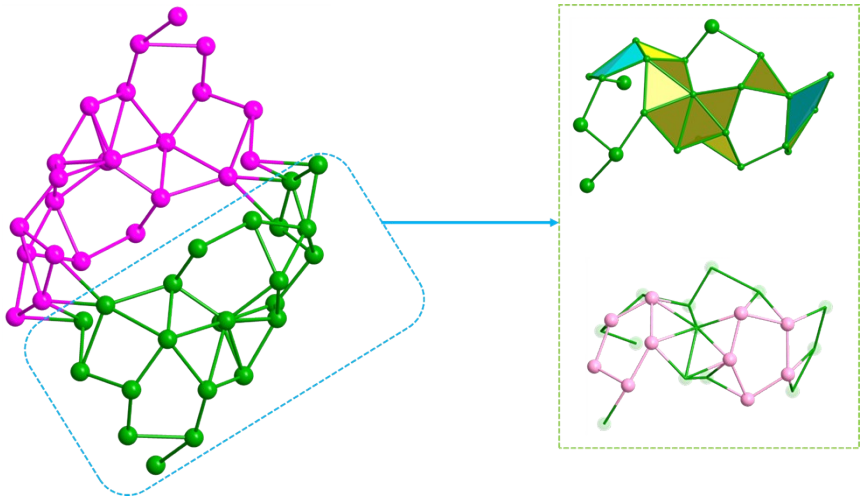

Fig. S13 The silver shell of the **Ag46** cluster. Left: overall structure; right: decomposition into Ag triangles (yellow), squares (blue), and pentagons (pink). Color codes: Ag, green, pink and purple.

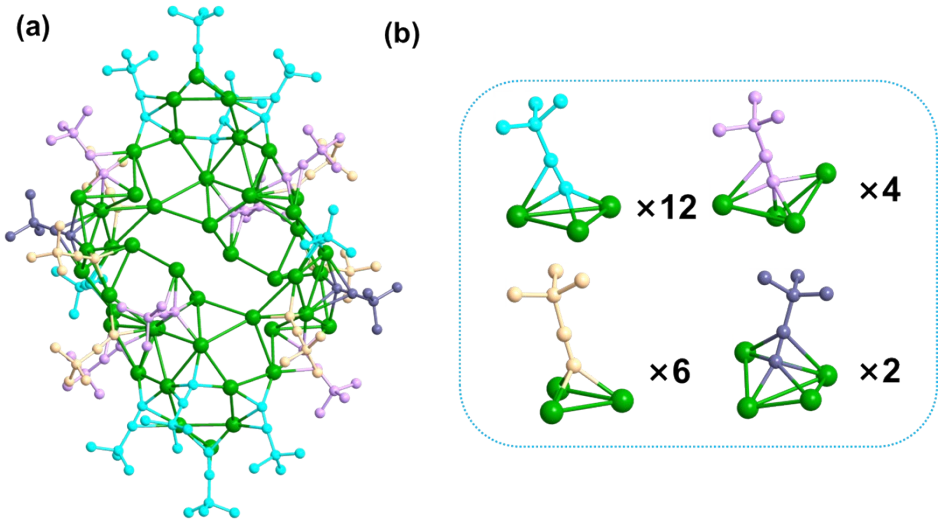

Fig. S14 (a) The 24 ^{t}BuC≡C^{-} ligands on the periphery of Ag_{46} shell. (b) the coordination modes of 24 ^{t}BuC≡C^{-} ligands: 12 in μ_3-η^1:η^1:η^2, 4 in μ_4-η^1:η^1:η^1:η^2, 6 in μ_3-η^1:η^1:η^1, 2 in μ_4-η^1:η^1:η^2:η^2. Color codes: Ag, green; C, yellow, gray, sky blue, purple.

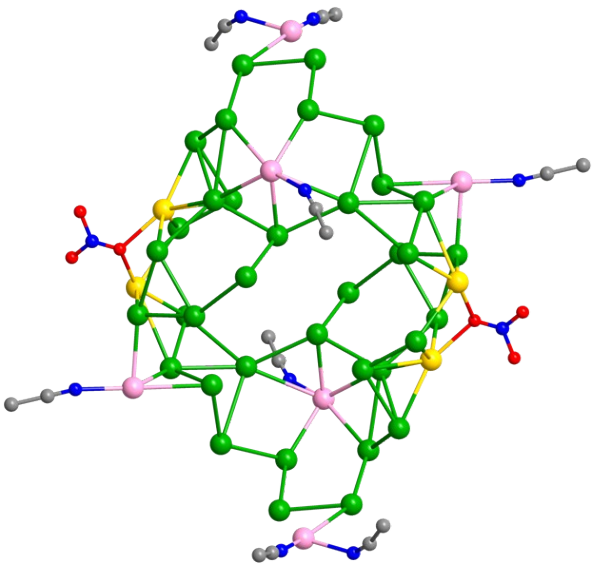

Fig. S15 The coordination modes of the CH_3CN molecules and NO_3^- ions within the **Ag46** cluster. Color codes: Ag, green, pink, yellow; C, grey; O, red; N, dark blue.

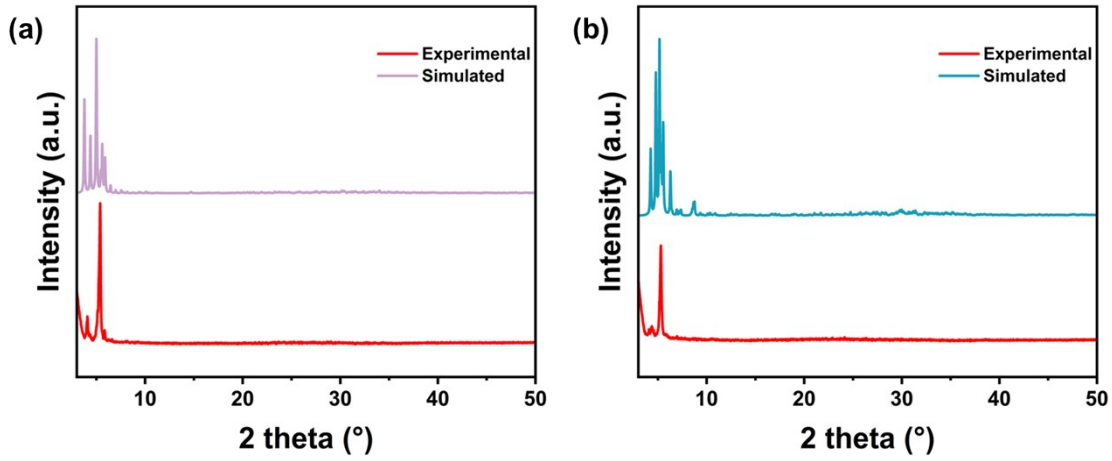

Fig. S16 Experimental and simulated PXRD patterns of (a) **Ag60** and (b) **Ag46**.

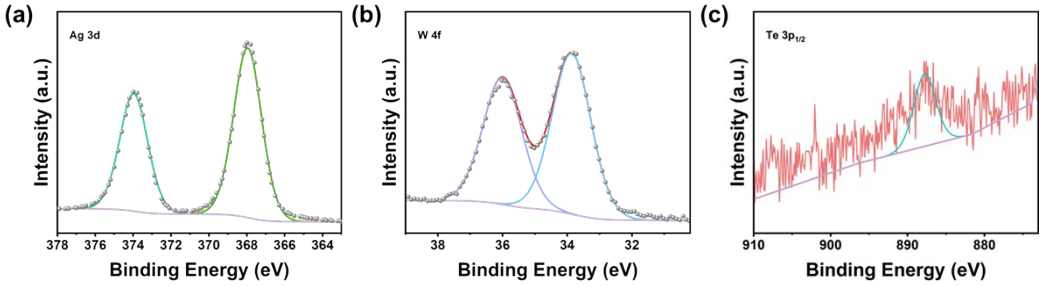

Fig. S17 High resolution XPS spectra of (a) Ag 3d, (b) W 4f, (c) Te $3p_{1/2}$ for **Ag60** cluster.

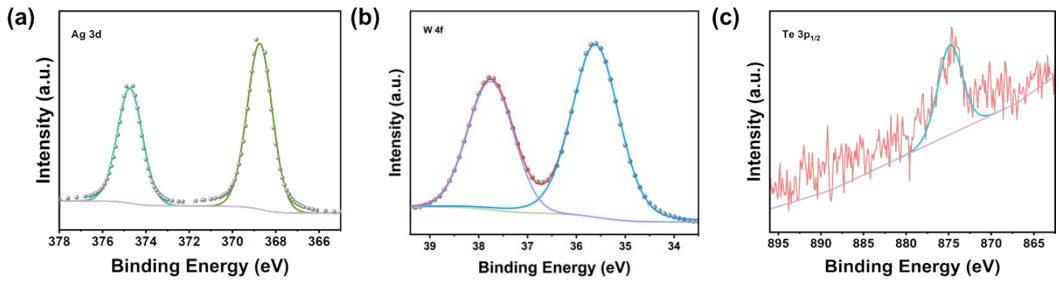

Fig. S18 High resolution XPS spectra of (a) Ag 3d, (b) W 4f, (c) Te $3p_{1/2}$ for **Ag46** cluster.

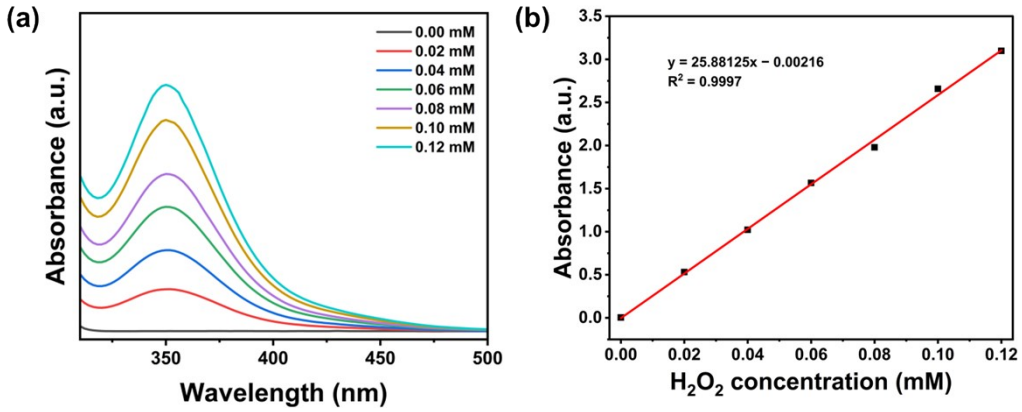

Fig. S19 (a) UV–vis absorption spectra of various H_2O_2 concentrations obtained via iodometric titration. (b) Corresponding calibration curve at the absorption peak of 350 nm. A known concentration of H_2O_2 solution was added to KI solution, and the change of absorption intensity at 350 nm was measured by UV–vis spectrometer.

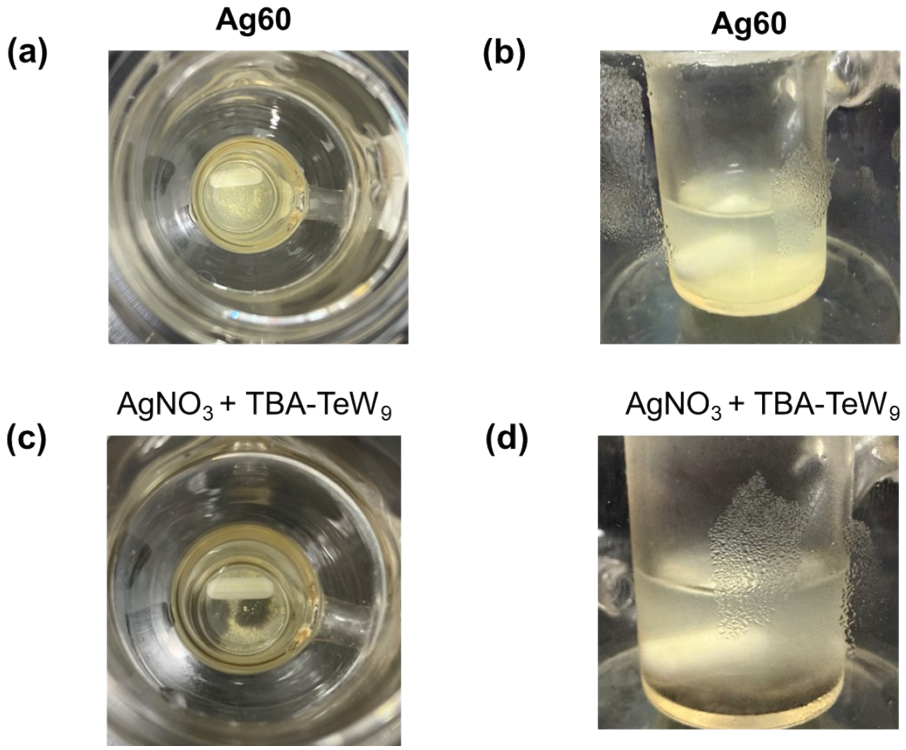

Fig. S20 Phenomenon of photocatalytic H_2O_2 production: (a) and (b) Photograph of the catalytic reaction solution after adding **Ag60**; (c) and (d) photograph of the catalytic reaction solution after adding $AgNO_3$ and TBA–TeW_9O_{33}.

Table S1. X-ray crystallographic data.

Identification code	**Ag60**	**Ag46**
Empirical formula	$C_{216}H_{324}Ag_{60}Cl_2N_{10}O_{78}Te_2W_{12}$	$C_{160}H_{240}Ag_{46}N_{10}O_{98}Te_2W_{26}$
Formula weight	13313.33	13868.93
Temperature/K	99.99(10)	100.00(10)
Crystal system	triclinic	triclinic
Space group	P-1	P-1
a/Å	19.0969(3)	18.8818(2)
b/Å	21.7033(4)	20.9962(2)
c/Å	25.4576(4)	21.4281(2)
α/°	71.606(2)	75.5420(10)
β/°	71.296(2	87.4930(10)
γ/°	72.725(2)	65.0760(10)
Volume/Å^3	9255.8(3)	7441.64(14)
Z	1	1
ρ_{calc}g/cm^3	2.388	3.095
μ/mm^{-1}	7.021	13.199
F(000)	6160.0	6244.0
Radiation	Mo Kα (λ = 0.71073)	Mo Kα (λ = 0.71073)
Index ranges	$-23 \le h \le 26$, $-28 \le k \le 29$, $-33 \le l \le 32$	$-26 \le h \le 27$, $-29 \le k \le 28$, $-30 \le l \le 28$
Reflections collected	122455	122122
Independent reflections	43838	38546
Data/restraints/parameters	43838/3/1426	38546/11/1054
Goodness-of-fit on F^2	1.031	1.046
Final R indexes [I>=2σ (I)]	R_1= 0.0599, wR_2= 0.1496	R_1= 0.0453, wR_2= 0.1125
Final R indexes [all data]	R_1= 0.1075, wR_2= 0.1805	R_1= 0.0652, wR_2= 0.1219

$$\boldsymbol{R_1} = \sum(|\boldsymbol{F_o}| - |\boldsymbol{F_c}|)/\sum|\boldsymbol{F_o}|,\ \mathbf{w}\boldsymbol{R_2} = \{\sum[\mathbf{w}(\boldsymbol{F^2_o} - \boldsymbol{F^2_c})^2]/\sum[\mathbf{w}(\boldsymbol{F^2_o})^2]\}^{1/2}$$

Table S2. Selected bond distances (Å) for **Ag60**.

Atom	Atom	Length/Å	Atom	Atom	Length/Å	Atom	Atom	Length/Å
W1	O40	2.223(7)	W5	O7	2.266(7)	Ag23	C18	2.366(14)
W1	O33	1.921(7)	W5	O33	1.897(8)	Ag23	C93	2.144(14)
W1	O29	1.939(7)	W5	O37	1.949(7)	Ag13	Ag22	2.9669(14)
W1	O34	1.743(12)	Ag8	O1	2.355(11)	Ag13	Cl1	2.484(4)
W1	O1	1.733(12)	Ag8	C72	2.213(13)	Ag13	O21	2.478(8)
W1	O10	2.226(7)	Ag8	C108	2.357(13)	Ag13	O34	2.343(11)
W2	O25	1.866(7)	Ag8	O6	2.541(7)	Ag13	C105	2.210(14)
W2	O38	2.167(7)	Ag28	Cl1	2.607(4)	Ag13	Ag2	2.9499(15)
W2	O21	1.983(7)	Ag28	O28	2.315(7)	Ag25	C55	2.480(15)
W2	O31	1.763(12)	Ag28	Ag18	3.0993(15)	Ag20	C57	2.207(13)
W2	O30	1.741(7)	Ag28	Ag4	2.9601(14)	Ag20	C15	2.201(12)
W2	O10	2.256(7)	Ag28	C52	2.160(14)	Ag20	C50	2.530(12)
W3	O38	2.246(7)	Ag30	Ag15	3.0464(15)	Ag20	C29	2.599(15)
W3	O28	2.254(7)	Ag30	C109	2.235(14)	Ag21	Ag17	3.2910(16)
W3	O21	1.900(8)	Ag30	C57	2.298(14)	Ag21	Ag29	3.2993(16)
W3	O35	1.930(8)	Ag30	C50	2.646(14)	Ag21	O20	2.541(12)
W3	O8	1.753(8)	Ag26	Ag24	2.9562(15)	Ag21	C34	2.299(13)
W3	O32	1.739(8)	Ag26	O36	2.388(11)	Ag21	C45	2.208(12)
W4	O37	1.925(7)	Ag26	C72	2.161(12)	Ag21	C58	2.664(15)
W4	O28	2.277(7)	Ag26	C15	2.283(12)	Ag14	Ag27	2.8974(16)
W4	O35	1.955(7)	Ag23	Ag27	3.1413(15)	Ag14	Ag29	3.2154(16)
W4	O16	1.769(9)	Ag23	Ag10	3.2578(17)	Ag14	C44	2.187(15)
W4	O5	1.742(8)	Ag23	O35	2.397(8)	Ag14	C33	2.282(15)
W4	O6	2.240(8)	Ag23	C72	2.255(13)	Ag14	C101	2.476(14)
Ag14	O5	2.483(8)	W5	O27	1.752(7)	Ag16	C44	2.251(14)
Ag11	Ag9	3.3406(16)	W5	O39	1.739(8)	Ag16	C73	2.423(14)
Ag11	Ag10	3.0447(16)	W5	O6	2.215(7)	Ag16	Ag4	3.2991(15)
Ag11	O9	2.579(12)	W6	O40	2.194(7)	Ag16	C104	2.170(13)
Ag11	C46	2.512(14)	W6	O25	1.936(7)	Ag7	Ag25	3.2071(16)
Ag11	C47	2.256(12)	W6	O7	2.242(7)	Ag7	O11	2.507(11)
Ag11	C1	2.186(14)	W6	O29	1.930(8)	Ag7	O22	2.564(11)
Ag9	Ag10	Ag9	W6	O26	1.746(7)	Ag7	Ag18	2.7349(14)
Ag9	Ag5	Ag9	W6	O36	1.729(12)	Ag7	Ag4	3.0935(16)
Ag9	C100	Ag9	Te	O40	1.906(7)	Ag7	C104	2.351(13)
Ag9	Ag2	Ag9	Te	O7	1.908(7)	Ag7	C9	2.648(18)
Ag9	C1	Ag9	Te	O38	1.956(7)	Ag7	C80	2.244(14)
Ag10	C93	2.171(17)	Te	O28	1.980(7)	Ag24	Ag20	2.9964(15)
Ag1	Ag4	2.9929(16)	Te	O10	1.904(7)	Ag24	O30	2.571(8)

Ag1	C42	2.392(14)	Te	O6	1.950(7)	Ag24	O8	2.541(8)
Ag1	C104	2.400(13)	Ag31	Ag30	2.9088(14)	Ag24	C15	2.129(13)
Ag1	O2	2.249(11)	Ag31	Ag24	3.1783(15)	Ag24	C46	2.572(13)
Ag18	Ag4	3.0518(16)	Ag31	Ag11	3.3115(14)	Ag24	C47	2.280(13)
Ag18	C52	2.287(16)	Ag31	Ag22	3.2350(15)	Ag15	Ag20	3.2393(15)
Ag18	C80	2.156(15)	Ag31	C109	2.122(15)	Ag15	O27	2.147(7)
Ag18	C103	2.544(16)	Ag31	C47	2.088(14)	Ag15	C57	2.064(14)
Ag12	Ag21	3.0969(14)	Ag8	Ag26	2.8072(14)	Ag25	Ag21	3.0041(16)
Ag12	Ag17	3.1249(15)	Ag8	Ag3	3.1407(14)	Ag25	Ag29	3.2531(17)
Ag12	O31	2.106(12)	Ag16	Ag19	3.2941(15)	Ag25	C45	2.073(17)
Ag12	C34	2.051(14)	Ag16	Ag1	2.9777(18)	Ag25	C80	2.203(16)
Ag16	Ag7	3.0972(15)	Ag16	O16	2.487(8)	Ag27	Ag10	3.3096(16)
Ag27	C44	2.134(14)	Ag22	Ag2	3.1716(15)	Ag3	C33	2.105(15)
Ag27	C93	2.181(15)	Ag17	Ag3	3.0648(16)	Ag19	Ag5	2.8663(17)
Ag22	C109	2.277(12)	Ag17	C34	2.229(14)	Ag19	Ag1	2.9310(17)
Ag22	C85	2.419(12)	Ag17	C108	2.236(13)	Ag19	O32	2.486(8)
Ag22	C105	2.147(15)	Ag17	C102	2.534(14)	Ag19	O16	2.470(9)
Ag5	Cl1	2.489(4)	Ag17	C58	2.591(14)	Ag19	O12	2.276(13)
Ag5	C100	2.180(16)	Ag29	C45	2.183(13)	Ag19	Ag4	3.0360(15)
Ag5	Ag2	3.0388(16)	Ag29	C33	2.193(16)	Ag19	C42	2.094(13)
Ag5	C42	2.396(14)	Ag2	C100	2.261(16)	Ag4	C42	2.488(14)
Ag10	C1	2.110(16)	Ag2	C87	2.607(18)	Ag4	C104	2.360(12)
O26	Ag18	2.352(8)	Ag4	C52	2.180(15)	Ag2	C105	2.209(16)

Table S3. Selected bond distances (Å) for **Ag46**.

Atom	Atom	Length/Å	Atom	Atom	Length/Å	Atom	Atom	Length/Å
W1	O51	2.218(6)	W5	O21	1.971(8)	W2	O26	2.220(8)
W1	O48	1.997(8)	W5	O38	1.817(7)	W2	O52	1.983(7)
W1	O30	2.100(6)	W5	O17	1.727(8)	W2	O18	1.916(7)
W1	O52	1.894(6)	W5	O33	2.310(7)	W2	O16	2.149(7)
W1	O50	1.764(6)	W5	O7	1.917(6)	W2	O49	1.771(7)
W1	O19	1.757(6)	W5	O42	1.992(8)	W2	O40	1.736(6)
W3	O51	2.189(6)	W4	O23	1.942(7)	W6	O7	1.924(7)
W3	O51	2.058(6)	W4	O18	1.949(7)	W6	O25	1.806(7)
W3	O48	1.948(8)	W4	O33	2.431(6)	W6	O29	1.736(7)
W3	O26	1.786(9)	W4	O42	1.895(9)	W6	O15	1.982(7)
W3	O30	1.877(6)	W4	O6	1.877(6)	W6	O2	2.005(6)
W3	O20	1.776(8)	W4	O39	1.704(8)	W6	O22	2.301(6)
W7	O12	1.932(6)	W8	O43	2.142(6)	W9	O43	1.876(6)
W7	O24	1.879(6)	W8	O24	2.040(7)	W9	O12	1.936(7)
W7	O5	1.939(6)	W8	O20	2.217(8)	W9	O47	1.912(6)
W7	O15	1.891(7)	W8	O4	1.798(7)	W9	O10	2.304(7)
W7	O22	2.386(7)	W8	O41	1.752(7)	W9	O44	1.916(6)
W7	O9	1.729(7)	W8	O8	1.813(7)	W9	O36	1.715(7)
W10	O23	1.903(7)	W11	O47	1.930(7)	W12	O46	1.886(7)
W10	O16	1.879(6)	W11	O35	1.901(7)	W12	O33	2.479(6)
W10	O45	1.944(7)	W11	O1	1.902(7)	W12	O1	1.913(7)
W10	O10	2.347(6)	W11	O45	1.919(7)	W12	O21	1.892(9)
W10	O44	1.938(7)	W11	O10	2.437(6)	W12	O6	1.931(6)
W10	O28	1.720(7)	W11	O31	1.707(8)	W12	O27	1.701(7)
W13	O5	1.899(7)	Te	O33	1.882(7)	Ag6	Ag15	2.9036(11)
W13	O46	1.924(7)	Te	O22	1.887(6)	Ag6	Ag7	2.9203(11)
W13	O35	1.922(7)	Te	O10	1.883(6)	Ag6	Ag16	3.2784(12)
W13	O2	1.872(7)	Ag12	O51	2.172(7)	Ag17	Ag3	3.3371(12)
W13	O22	2.467(6)	Ag12	O49	2.541(7)	Ag17	Ag14	2.9006(12)
W13	O11	1.719(6)	Ag12	C63	2.130(16)	Ag17	Ag7	2.9824(12)
Ag1	Ag11	2.9065(10)	Ag6	O48	2.358(9)	Ag17	Ag20	3.1921(12)
Ag1	Ag3	2.9145(11)	Ag6	O38	2.308(7)	Ag17	Ag22	3.3411(15)
Ag1	Ag14	3.0003(11)	Ag6	O25	2.362(7)	Ag17	O4	2.228(7)
Ag1	O30	2.349(6)	Ag6	C81	2.171(15)	Ag17	C63	2.365(15)
Ag1	O43	2.504(6)	Ag8	Ag19	2.9443(11)	Ag17	C18	2.143(15)
Ag1	O16	2.598(7)	Ag8	Ag24	3.0116(11)	Ag11	Ag14	3.2307(12)
Ag4	Ag8	2.9806(10)	Ag8	C27	2.324(15)	Ag11	Ag2	2.9468(12)
Ag4	Ag18	3.0110(12)	Ag8	C66	2.414(15)	Ag11	C30	2.165(15)
Ag4	Ag9	3.0795(11)	Ag8	C58	2.298(16)	Ag11	C46	2.282(15)
Ag4	O24	2.514(6)	Ag12	Ag17	2.8762(11)	Ag11	C65	2.690(15)
Ag4	O50	2.473(6)	Ag12	Ag24	3.1826(12)	Ag15	Ag7	3.1370(12)

Ag4	O25	2.316(7)	Ag12	Ag16	2.8387(12)	Ag15	Ag2	3.0930(12)
Ag4	C27	2.223(15)	Ag12	Ag22	3.0259(13)	Ag15	Ag9	2.8579(12)
Ag19	Ag24	3.3302(11)	Ag19	C69	2.657(15)	Ag15	C81	2.162(16)
Ag19	Ag2	2.9191(12)	Ag24	Ag18	3.3798(12)	Ag15	C66	2.123(16)
Ag19	O40	2.600(7)	Ag24	Ag22	3.3341(13)	Ag21	Ag10	3.0022(12)
Ag19	C30	2.261(15)	Ag21	C24	2.158(15)	Ag21	Ag20	2.9840(12)
Ag19	C58	2.160(15)	Ag21	C15	2.332(15)	Ag21	Ag5	3.1975(13)
Ag10	Ag13	3.023(2)	Ag21	C75	2.542(15)	Ag21	O41	2.597(7)
Ag10	O41	2.477(7)	Ag10	O9	2.494(7)	Ag21	O36	2.491(8)
Ag10	C24	2.180(15)	Ag20	Ag22	3.2701(15)	Ag7	C81	2.133(15)
Ag10	C60	2.343(15)	Ag20	C29	2.241(15)	Ag7	C18	2.151(15)
Ag10	C20	2.469(15)	Ag20	C15	2.137(15)	Ag16	O18	2.521(6)
Ag10	Ag23	3.182(11)	Ag20	C23	2.568(16)	Ag16	O38	2.188(7)
Ag24	O50	2.538(7)	Ag5	N6	2.171(16)	Ag16	C63	2.290(15)
Ag24	O8	2.322(7)	Ag5	C24	2.250(16)	Ag16	C70	2.468(15)
Ag24	C58	2.249(15)	Ag5	C78	2.600(16)	Ag9	O29	2.485(7)
Ag24	O49	2.513(7)	Ag5	N4	2.276(9)	Ag9	C27	2.381(16)
Ag3	Ag20	3.0267(12)	Ag22	Ag13	2.840(3)	Ag9	C66	2.644(15)
Ag3	C46	2.266(15)	Ag18	Ag13	2.930(5)	Ag9	N5	2.283(11)
Ag3	C15	2.141(15)	Ag18	C27	2.238(15)	Ag14	C18	2.278(16)
Ag14	Ag7	2.9211(12)	Ag18	C60	2.129(15)	Ag2	O32	2.424(10)
Ag14	O19	2.542(7)	Ag18	C21	2.549(15)	Ag2	C30	2.133(16)
Ag14	O32	2.330(9)	Ag18	Ag23	3.337(17)	Ag2	C66	2.289(15)
Ag14	C46	2.220(16)	Ag23	C23	2.690(19)	Ag2	C47	2.615(15)
Ag13	C60	2.116(16)	Ag22	C63	2.276(15)	Ag22	Ag23	3.056(11)
Ag13	C29	2.175(16)	Ag22	C29	2.138(15)	Ag22	N2	2.333(10)
Ag23	C60	2.196(18)	Ag23	C29	2.079(17)			

Table S4. BVS values for W and Te atoms of **Ag60**.

W1	6.047	W4	5.773
W2	6.019	W5	5.989
W3	6.001	W6	6.054
Te	5.749		

Table S5. BVS values for W and Te atoms of **Ag46**.

W1	5.976	W7	6.027
W2	5.930	W8	5.972
W3	6.085	W9	6.161
W4	6.055	W10	6.037
W5	6..008	W11	6.055
W6	5.944	W12	6.143
W13	6.081	Te	3.857

Table S6. Comparison of photocatalytic H_2O_2 production among recently reported materials.

Samples	Solutions	[Cat.]/ g L^{-1}	Light	H_2O_2 yield μmol g^{-1} h^{-1}	Ref.
Ag60	10 % vol IPA	0.2	Xenon lamp	6752.1	**This**
Ag46	10 % vol IPA	0.2	Xenon lamp	5334.2	**Work**
CityU-40	Pure water	1	λ = 380~1100	342.5	**This**
TF_{50}-COF	10 % vol Ethanol	0.1	nm	1739	**Work**
Ag@U-g-C_3N_4	Pure water	1	λ ≥ 400 nm	24.84	4
$W_{18}O_{49}$@g-C_3N_4	Pure water	0.2	Xenon lamp	71	5
DDCN	Pure water	0.2	λ ≥ 400 nm	192	6
PEI/C3N4	Pure water	1	λ ≥ 420 nm	208	7
Cv-g-C_3N_4	Pure water	1	AM 1.5G	92	8
ACN	10 % vol IPA	0.5	λ ≥ 400 nm	1874	9
Py-OH-Sa-COF	10 % vol IPA	0.1	λ ≥ 420 nm	4780	10
fl-CN-530	10 % vol Ethanol	0.5	full spectrum	952.3	11
			λ ≥ 420 nm		12
					13

References

1. O. V. Dolomanov, L. J. Bourhis, R. J. Gildea, J. A. K. Howard and H. Puschmann, OLEX2: a complete structure solution, refinement and analysis program, *J. Appl. Crystallogr.*, 2009, **42**, 339-341.
2. G. Sheldrick, Combining biophysical methods for the analysis of protein complex stoichiometry and affinity in SEDPHAT, *Acta Crystallogr. Sect. C*, 2015, **71**, 3-8.
3. N. E. Brese and M. O'Keeffe, Bond-valence parameters for solids, *Acta Crystallogr. Sect. B*, 1991, **47**, 192-197.
4. L. Zhang, Z. Chen, X.-X. Li, X. Wang, Q. Gu, Z. Zheng, N. Aratani, C.-S. Lee, Y.-Q. Lan and Q. Zhang, Constructing Dual-Functional Organic Cuboctahedron Cages with Two Different Triangular Building Units for Efficient Artificial Photosynthesis of Hydrogen Peroxide from Water and Oxygen, *J. Am. Chem. Soc.*, 2025, **147**, 27847-27854.
5. H. Wang, C. Yang, F. Chen, G. Zheng and Q. Han, A Crystalline Partially Fluorinated Triazine Covalent Organic Framework for Efficient Photosynthesis of Hydrogen Peroxide, *Angew. Chem. Int. Ed.*, 2022, **61**, e202202328.
6. J. Cai, J. Huang, S. Wang, J. Iocozzia, Z. Sun, J. Sun, Y. Yang, Y. Lai and Z. Lin, Crafting Mussel-Inspired Metal Nanoparticle-Decorated Ultrathin Graphitic Carbon Nitride for the Degradation of Chemical Pollutants and Production of Chemical Resources, *Adv. Mater.*, 2019, **31**, 1806314.
7. X. Li, F. Ye, H. Zhang, M. Ahmad, Z. Zeng, S. Wang, S. Wang, D. Gao and Q. Zhang, Ternary rGO decorated $W_{18}O_{49}$@g-C_3N_4 composite as a full-spectrum-responded Z-scheme photocatalyst for efficient photocatalytic H_2O_2 production and water disinfection, *J. Environ. Chem. Eng.*, 2023, **11**, 110329.
8. G. Ba, H. Hu, F. Bi, J. Yu, E. Liu, J. Ye and D. Wang, Engineering nitrogen vacancies and cyano groups into C_3N_4 nanosheets for highly efficient photocatalytic H_2O_2 production, *Appl. Catal. B*, 2025, **361**, 124645.
9. X. Zeng, Y. Liu, Y. Kang, Q. Li, Y. Xia, Y. Zhu, H. Hou, M. H. Uddin, T. R. Gengenbach, D. Xia, C. Sun, D. T. McCarthy, A. Deletic, J. Yu and X. Zhang, Simultaneously Tuning Charge Separation and Oxygen Reduction Pathway on Graphitic Carbon Nitride by Polyethylenimine for Boosted Photocatalytic Hydrogen Peroxide Production, *ACS Catal.*, 2020, **10**, 3697-3706.
10. S. Li, G. Dong, R. Hailili, L. Yang, Y. Li, F. Wang, Y. Zeng and C. Wang, Effective photocatalytic H_2O_2 production under visible light irradiation at g-C_3N_4 modulated by carbon vacancies, *Appl. Catal. B*, 2016, **190**, 26-35.
11. Y. Zheng, Y. Luo, Q. Ruan, S. Wang, J. Yu, X. Guo, W. Zhang, H. Xie, Z. Zhang and Y. Huang, Plasma-induced hierarchical amorphous carbon nitride nanostructure with two N_2C-site vacancies for photocatalytic H_2O_2 production, *Appl. Catal. B,* 2022, **311**, 121372.
12. P. Huang, Y.-Y. Peng, X.-H. Wang, R.-H. Li, M.-H. Qin, M. Zhang, S.-M. Wang, M. Lu, S.-L. Li and Y.-Q. Lan, Charge-Distribution and Microenvironment Dual Regulation of Covalent Organic Frameworks for Enhancing Photocatalytic H_2O_2 and H_2 Production, *Adv. Mater.,* 2026, **38**, e07849.
13. B. Feng, Y. Liu, K. Wan, S. Zu, Y. Pei, X. Zhang, M. Qiao, H. Li and B. Zong, Tailored Exfoliation of Polymeric Carbon Nitride for Photocatalytic H_2O_2 Production and CH_4 Valorization Mediated by O_2 Activation, *Angew. Chem. Int. Ed.,* 2024, **63**, e202401884.